Electron Attachment to Helium Microdroplets: Creation Induced Magic?

T. Jiang, C. Kim, and J. A. Northby
Physics Department, University of Rhode Island, Kingston, Rhode Island 02881
(Received 18 March 1993)

The size distribution of He_N^- ions produced by crossing a low energy electron beam with an uncharged helium cluster beam exhibits a threshold below which no ions are detected. The threshold region is unexpectedly structured, however, and exhibits a sharp "magic" mass peak at $N=(2.0 \pm 0.1)\times 10^5$ atoms. We suggest that this behavior derives from the dynamics of the conduction band instability which leads to the formation of a metastably trapped bubble electron in the droplet.

PACS numbers: 36.40.+d, 34.80.−i, 67.40.Yv, 72.90.+y

The dominant interaction between an electron and a helium atom is a strongly repulsive short range one, and as a result the conduction band for an excess electron in uniform density liquid helium lies about $V_0 \sim 1$ eV above the vacuum level [1-3]. The delocalized state is highly unstable, however, and rapidly decays to a localized "bubble" state [1,4,5] in which the electron is confined to a cavity in the liquid of radius about 17 Å. There is in addition a much weaker long range attractive polarization interaction which both draws an exterior electron towards and repels an interior electron from the helium-vacuum interface. This attraction results in the well studied exterior 2D surface electron states [1,6,7] as well as in the observed barrier to extraction of negative carriers from helium into the vacuum [1,8,9]. It has been suggested [10-12] that an exterior surface electron bound state should also exist on a finite helium droplet as long as it was larger than a threshold size variously estimated to lie in the range $N=2\times 10^5$ [12] to $N=5\times 10^5$ atoms [11]. Large ($>2\times 10^6$ atoms) negatively charged helium droplets were first observed by Gspaan [13], who attributed their structure to these exterior bound states. More recently we have also reported [14,15] measurements of negatively charged helium droplets ($>5\times 10^5$ atoms). The apparent threshold was suggestively close to that predicted by the exterior electron model, but we observed a stability in electric fields which appeared to be in conflict with it. We proposed an alternative model in which the electron is located in an interior bubble state which is confined near the center of the droplet by the above mentioned polarization attraction. While this state is only metastable, nonetheless even charged droplets as small as $\sim 3\times 10^4$ atoms should be stable on experimental time scales in fairly strong electric fields [16].

In the experiments to be discussed here we have examined the threshold for production of He_N^- ions by low energy electron attachment to neutral helium droplets, in significantly more detail than previously possible. The improvements derive mostly from a more sensitive detection scheme in which electrons are detached from droplets by surface collisions and counted with an electron multiplier. The experimental method is indicated schematically in Fig. 1. Highly purified He gas in a stagnation chamber at low temperatures ($T_0=5$-10 K) and high pressures ($P_0=10$-80 bars) expands through a 5 μm sonic nozzle, NZ, into a vacuum ($P_1 < 10^{-3}$ torr). The resulting supercritical expansion cools adiabatically, becoming a superheated liquid. The liquid then fragments, producing both monomers and neutral droplets whose sizes range from below 10^4 atoms to more than 10^7 atoms [14,15]. The expansion next passes through a skimmer, SK, into a high vacuum chamber ($P_2=10^{-6}$ torr), and axially through an electron attachment cell C which is held at ground potential. Electrons emitted from heated filaments F are accelerated through a control grid G and then decelerated before they pass radially through mesh covered openings in the wall of the cell. The neutral droplet velocity distribution is narrow with an energy per atom of about 1 meV. The droplets are thus quite energetic and are not significantly deflected by the electron attachment process. The resulting He_N^- beam is further collimated by a 1.5 mm aperature S and enters the analyzing and detection region. Two detectors, a Faraday collector FC and a channel electron multiplier (CEM), are mounted on a movable arm 44 cm from S. Either may be positioned a variable distance d (~ 2 cm) off the beam axis. The collimating aperature at the CEM is 1.5 mm in diameter and is followed by a 50% transmitting grid. We believe that ions which strike this grid release their electrons, some of which are accelerated into the CEM and counted, but the precise detection mechanism is not known. The ions passing through S are deflected by a transverse electric field E_d and reach the detector only if they have energy $E=K_0(E_d/d)$, where

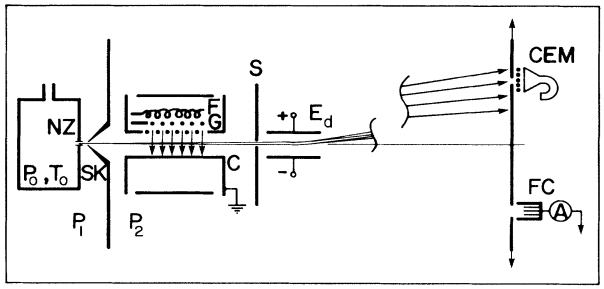

FIG. 1. Apparatus schematic showing droplet source, electron attachment cell, energy-velocity analyzer, and detectors.

0031-9007/93/71(5)/700(4)$06.00

K_0 is a geometrical constant. The Faraday collector response as a function of E_d gives us the ion energy distribution directly. In the CEM case the distribution is folded with the detector response function which, while it is not known *a priori,* we expect to be a smoothly decreasing function of droplet mass. Despite this uncertainty, the CEM remains our primary detector because its higher sensitivity and rapid response allows us to measure with higher energy resolution, and also to obtain the ion velocity by a time of flight measurement. (Since there are no significant axial fields we simply gate the electron beam with the control grid G and measure the time delayed pulse at the detector with signal averaging techniques.)

Figure 2 shows a typical energy spectrum obtained with the CEM detector for fixed stagnation conditions. The main curve was obtained by recording the analog output of a counting rate meter while sweeping the deflection voltage. The axis is calibrated in terms of the ion energy E. The most striking feature of this curve is the sharp peak at low energies, below which the ion current vanishes. It is quite narrow, since about 50% of the observed width comes from the finite resolution of the energy analyzer. The inset shows this peak measured much more carefully by a point by point method with 100 s of integration at each point. Its central energy is well defined, and depends on the stagnation conditions. This dependence is shown in Fig. 3(a), where we plot the energy of the peak as a function of stagnation temperature for various stagnation pressures. Figure 3(b) shows the velocity of the ions at the energy peak measured under those same conditions. Figure 3(c) shows the mass of the peak ions extracted from these data. It is clear that the peak corresponds to a particular ion mass, and not to a particular energy. Furthermore, this particular "magic" size $[(2.0 \pm 0.1) \times 10^5$ atoms] is a property of the ion beam and not the precursor neutral beam, whose size distribution is strongly dependent on the stagnation conditions. It should be emphasized that this is not simply a size resonance in a fixed energy capture cross section. We mix together fairly broad and variable electron energy distributions with very broad and variable droplet mass distributions and get out a strongly favored charged droplet mass. To help convince ourselves that the peak is not some artifact of the apparatus we have checked that the results can be reproduced for different signs and magnitudes of the detector displacement d. Also, since helium droplets easily capture background gas atoms [17,18], we increased the background pressure by adding a small leak. If such impurities were an essential factor in the capture process we would expect the signal amplitude to increase. In fact, we observed a slight decrease. Finally, to check that a rapid variation in the CEM detector sensitivity near the mass threshold is not responsible for the effect, we have replaced the CEM by the Faraday collector. While the resolution and signal to noise ratio were significantly worse, the peak was still clearly visible.

The observation of magic charged cluster sizes is common [19–24]. They are normally interpreted as a

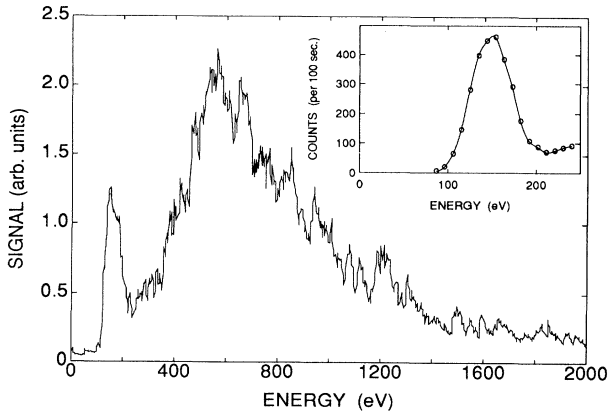

FIG. 2. Energy spectrum measured with the CEM detector by sweeping E_d at $P_0 = 20.7$ bars, $T_0 = 9.5$ K. Inset shows low energy peak at higher resolution.

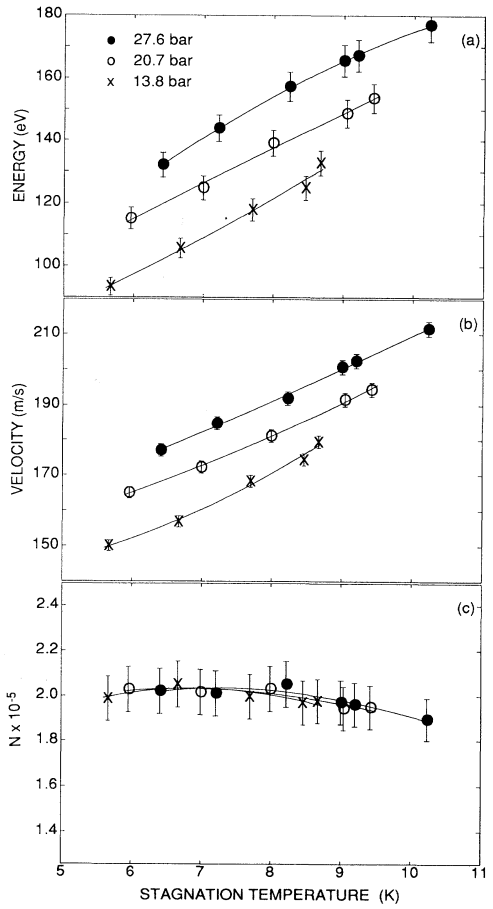

FIG. 3. (a) Low energy ion peak position vs stagnation temperature at three different pressures. (b) Velocity of ions at the peak measured under identical conditions. (c) Mass of ions at the peak calculated from (a) and (b).

reflection of some special stability of a particular cluster size relative to its neighbors such as, for example, those associated with electronic or geometrical shell closings. It is difficult, however, to imagine any such special stabilities associated with the large, presumably liquid droplets in question here. It is easy to understand a stability threshold for electron attachment, but not a stability peak. Instead, we propose that this is a new kind of "magic" which derives from the process of creation of a trapped bubble electron in the droplet. The qualitative argument goes as follows: Since the bubble is not present in the droplet before the collision with the electron, it must be created as part of the collision process. The mechanism of the conduction band instability that leads to bubble formation in the bulk liquid is fairly clear. The strongly repulsive electron-helium interaction drives the atoms toward regions where the electron probability density is low and the reaction force increases the electron probability where the helium density is low. Any departures from uniformity are then amplified. Little is known in detail about the dynamics of the process [25,26], but since it involves the cooperative motion of a large number of helium atoms it must take some time. A reasonable rough estimate of the characteristic time for bubble formation t_b is obtained from the ratio of the bubble radius ($R_b \sim 17$ Å) to the speed of sound ($v_s \sim 240$ ms/s), giving $t_b \sim 0.7\times10^{-11}$ s. Consequently, if an electron is to be captured into a bubble state it must remain inside the droplet for a time of this order so that the bubble has time to develop. If we treat the collision between a low energy electron and a droplet in the adiabatic approximation for times much shorter than t_b (i.e., clamp the atoms), the effective potential seen by the electron is, in first approximation, simply a spherical potential barrier of height V_0, as sketched in Fig. 4(a). There are many scattering resonances in this potential associated with states whose wavelength in the conduction band is commensurate with the droplet radius. A typical example ($n=1$, S-wave resonance) is also sketched in the figure. It is straightforward to evaluate the energies E_r and lifetimes T_d of the S-wave resonances in this potential as a function of the droplet radius R_c, obtaining

$$E_r = (\hbar^2/2mR_c^2)(n\pi)^2 + V_0\,,$$
$$T_d = \hbar/\Gamma = (n\pi\hbar/4)E_r^{1/2}/(E_r - V_0)^{3/2}\,, \tag{1}$$

where Γ is the resonance width in energy (FWHM). Assuming bulk liquid density, $R_c(\text{Å}) = 2.22(N)^{1/3}$, and the observed magic size corresponds to $R_c = 130$ Å. The longest lived resonance in this case ($n=1$) lies 2.2×10^{-3} eV above the bottom of the conduction band and its lifetime is 0.49×10^{-11} s. Since this is quite close to t_b the adiabatic approximation is no longer valid. Instead, we expect that if this state is excited in the collision, deformation and capture of the electron into a bubble state will probably occur. The reason that this formation mechanism produces a peak and not simply a threshold is less obvious. A qualitative explanation is that when the droplet is much smaller than 130 Å, the resonance is broad and can be excited by electrons with relatively wide range of energies. The lifetime is short, however, and the electrons escape before a bubble can form. When the drop is much larger than 130 Å, the lifetime is long enough, but the resonance is very narrow and only very few electrons have the correct energy to excite it. Thus when a broad droplet size distribution is mixed with electrons whose energy distribution is also broad we would expect to produce ions preferentially from droplets whose resonance lifetime is just equal to the time required for the instability to set in.

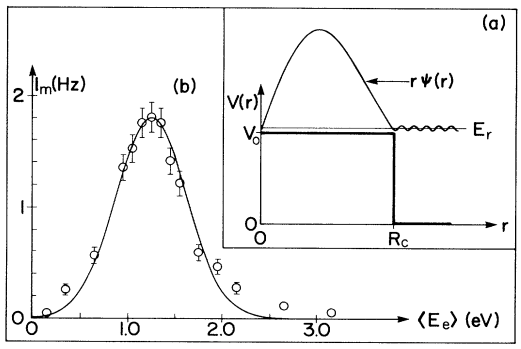

FIG. 4. (a) Sketch of the resonant ($n=1$, S-wave) electron wave function [$r\Psi(r)$] in the effective adiabatic potential of the drop. (b) Measured amplitude of the "magic droplet" signal as a function of the mean electron energy ⟨E_e⟩ in the attachment cell.

Since this argument predicts that the only electrons which can be captured are those whose energies lie in a narrow range just above the bottom of the conduction band, we have studied how the magic droplet signal depends on the electron energy. Our electron source was not designed to produce a monoenergetic electron beam, but we have found that if we operate at low heater voltage to eliminate space charge fields we can obtain a symmetric energy distribution whose FWHM is less than 1 eV and whose mean energy ⟨E_e⟩ can be independently controlled by the filament voltage. The experimental variation of the magic signal with ⟨E_e⟩ is shown in Fig. 4(b). The signal has a maximum when the mean electron energy equals 1.2 eV, which is very close to most measured values [2] of V_0. Furthermore, most of the width of this curve can be accounted for by the spread in electron energies, with the implication that the energy dependence of the attachment cross section itself is very sharp.

Up to this point we have not discussed the origin of the second peak in Fig. 2 at larger masses. Because it is broad, its apparent location is determined more by the dropoff in CEM detector sensitivity with increasing mass than by the mass distribution itself. Certainly, as the

droplet size continues to increase beyond threshold, we would expect other higher resonances to satisfy the condition $T_d = t_b$ as well. For example, from Eq. (1) we see that $T_d \approx R_c^3/n^2$, so that the $n=2$, S-wave resonance will have the correct lifetime for droplets with 4 times the mass of the magic peak. It is clear, however, that there must also be other mechanisms which can produce electron attachment to very large droplets, since bubble formation takes place at bulk helium surfaces where the resonance process does not occur. Our only experimental information on this point is that the electron energy response curve, similar to Fig. 4(b) but for formation of the larger charged droplets, is slightly skewed towards higher energies. This indicates that additional mechanisms do exist for attachment of more energetic electrons to very large drops.

The model we have presented to explain the origin of the magic peak is at best semiquantitative, but we believe that it contains the essential physical mechanisms. A complete theory will necessarily involve the detailed dynamics of the bubble formation process, and should explain not only the location of the peak, but also its relatively narrow width. Probably the most important qualitative conclusion we can draw from these experiments is that the structure of the charged complex is almost certainly a bubble electron metastably trapped in the droplet. As such it will be optically active, readily detectable by electron detachment, and should provide a very convenient and useful probe of the dynamics of this unconfined microscopic superfluid system in the future.

This work was supported by the NSF (DMR8816482 and DMR9217525).

[1] A. L. Fetter, in *The Physics of Liquid and Solid Helium*, edited by K. H. Bennemann and J. B. Ketterson (Wiley, New York, 1976), Pt. 1, p. 207, and references therein.

[2] J. R. Broomall, W. D. Johnson, and D. G. Onn, Phys. Rev. B **14**, 2919 (1976).

[3] K. Martini, J. P. Toennies, and C. Winkler, Chem. Phys. Lett. **178**, 429 (1991).

[4] G. Careri, F. Scaramuzzi, and J. O. Thompson, Nuovo Cimento **13**, 186 (1959).

[5] C. C. Grimes and G. Adams, Phys. Rev. B **41**, 6366 (1990); **45**, 2305 (1992).

[6] M. W. Cole and M. H. Cohen, Phys. Rev. Lett. **23**, 1238 (1969).

[7] A. J. Dahm and W. F. Vinen, Phys. Today **40**, No. 2, 43 (1978).

[8] W. Schoepe and G. W. Rayfield, Phys. Rev. A **7**, 2111 (1973).

[9] M. W. Cole and J. R. Klein, J. Low Temp. Phys. **36**, 331 (1979).

[10] M. S. Khaikin, Pis'ma Zh. Eksp. Teor. Fiz. **27**, 706 (1978) [JETP Lett. **27**, 668 (1978)].

[11] M. V. Rama Krishna and K. B. Whaley, Phys. Rev. B **38**, 11839 (1988).

[12] T. M. Sanders, Jr. (to be published).

[13] J. Gspann, Physica (Amsterdam) **169B**, 519 (1991).

[14] T. Jiang and J. A. Northby, Phys. Rev. Lett. **68**, 2620 (1992).

[15] T. Jiang, S. Sun, and J. A. Northby, in *Physics and Chemistry of Finite Systems: From Clusters to Crystals*, edited by P. Jena *et al.* (Kluwer Academic, The Netherlands, 1992), Vol. 1, p. 223.

[16] We have extended the model of Schoepe and Rayfield (Ref. [11]) to a bubble electron in a droplet, using their measured tunneling probabilities [C. Kim, T. Jiang, and J. A. Northby (to be published)].

[17] A. Scheidemann, J. P. Toennies, and J. A. Northby, Phys. Rev. Lett. **64**, 1899 (1990).

[18] S. Goyal, D. L. Schutt, and G. Scoles, Phys. Rev. Lett. **69**, 933 (1992).

[19] O. Echt, K. Sattler, and E. Recknagel, Phys. Rev. Lett. **47**, 1121 (1981).

[20] M. L. Cohen, M. Y. Chou, W. D. Knight, and W. A. deHeer, J. Phys. Chem. **91**, 3141 (1987).

[21] I. A. Harris, R. S. Kidwell, and J. A. Northby, Phys. Rev. Lett. **53**, 2390 (1984).

[22] R. Casero, and J. M. Soler, J. Chem. Phys. **95**, 2927 (1991).

[23] C. E. Klots, Z. Phys. D **21**, 335 (1991).

[24] P. Stampfli and K. H. Bennemann, Phys. Rev. Lett. **69**, 3471 (1992).

[25] J. P. Hernandez and M. Silver, Phys. Rev. A **2**, 1949 (1970); **3**, 2152 (1971); J. P. Hernandez and S. Choi, Phys. Rev. **188**, 340 (1969). See also Ref. [2] and references therein.

[26] Three characteristics times are involved [25] in hot electron thermalization in bulk helium: the time to find and localize on a density defect ($\sim 10^{-12}$ s), the time to expand it into a bubble ($\sim 10^{-11}$ s), and the time to relax the electron bubble to its ground state ($\sim 10^{-10}$ s). In the cluster case the first is not relevant, since the cluster itself is the density anomaly. Metastable capture is presumably accomplished in the second step. It is possible that re-emission in the third step plays a significant role in determining the final distribution, however.